PROCEEDINGS OF SCIENCE

Interstellar gas in 3D, implications for CR propagation and gamma-ray emission

Guðlaugur Jóhannesson*
Science Institute, University of Iceland, Reykjavik, IS-105, Iceland and Nordita, KTH Royal Institute of Technology and Stockholm University, Roslagstullsbacken 23, SE-106 91 Stockholm, Sweden
E-mail: gudlaugu@hi.is

Igor V. Moskalenko
Hansen Experimental Physics Laboratory and Kavli Institute for Particle Astrophysics and Cosmology, Stanford University, Stanford, CA 94305, U.S.A.
E-mail: imos@stanford.edu

Troy A. Porter
Hansen Experimental Physics Laboratory and Kavli Institute for Particle Astrophysics and Cosmology, Stanford University, Stanford, CA 94305, U.S.A.
E-mail: tporter@stanford.edu

Cosmic-ray (CR) particles propagating in the Galaxy interact in the interstellar medium with gas, losing energy and producing secondary particles via inelastic losses and fragmentation. Observations of the secondaries can be used to constrain the origin and propagation of the CRs, and may also provide signatures of new physics. To date CR propagation models have used the 2D Galactocentric cylindrical symmetry approximation for the spatial distribution of the interstellar gas. This is partly due to difficulties in uniquely determining its true 3D structure. In this contribution a method for determining the 3D spatial distribution of interstellar gas is described and first results using it to develop models that can be used in CR propagation codes like *GALPROP* are given. Implications for analysis of CR and γ-ray data using 3D spatial models for the interstellar gas are also discussed.

35th International Cosmic Ray Conference
10-20 July, 2017
Bexco, Busan, Korea

*Speaker.

PoS(ICRC2017)871

1. Introduction

Cosmic rays (CRs) of all species are pervasive in the Galaxy. While propagating in the interstellar medium (ISM) they scatter off the turbulent magnetic field in a stochastic process that can be well described by diffusion (e.g. [1]). The CRs also interact with the gas in the ISM, producing secondary CR species and also electromagnetic radiation from radio to high-energy γ-rays. These secondary particles and electromagnetic emissions provide important information about the origin and propagation of CRs in our Galaxy (e.g., [2]). The production of these secondaries and emissions depends on the characteristics of the primary CRs and the ISM density distributions. Consequently, deciphering the origin of the CRs using the high-quality data available these days from instruments such as *Fermi*–LAT, PAMELA, and AMS-02 necessitates understanding as accurately as possible the spatial distribution of ISM densities. Until now almost all models of CR propagation have used two-dimensional (2D) azimuthally distributions of the ISM. In this proceedings a method is described to constrain the three-dimensional (3D) structure of interstellar gas in the Galaxy and preliminary results using the method are given. The effect on the generation of secondary CR particles in the Galaxty using the more realistic 3D models that are developed using the *GALPROP* propagation code is also discussed. For similar work for the 3D spatial distribution of the Galactic interstellar radiation field see [3].

Knowledge of the distribution of interstellar gas comes mostly from observation of the H I 21-cm line and CO 2.6-cm line (e.g. [4]). The attractiveness of the 21-cm line as a gas tracer is that the line emission can be directly related back to atomic hydrogen density if the excitation temperature is known. Under the assumption of a uniform excitation temperature, the radiative transport equation is [5] $T_B(v) = T_{BG}e^{-\tau(v)} + T_S(v)\left(1-e^{-\tau(v)}\right)$, where $T_B(v)$ is the observed brightness temperature, T_{BG} is the background temperature, $T_S(v)$ is the spin temperature, and $\tau(v) = N_{HI}(v)/(CT_S(v))$ is the line optical depth. Knowing $T_S(v)$ and T_{BG} observations of $T_B(v)$ can be used to determine $N_{HI}(v)$. Unfortunately, $T_S(v)$ can only be determined if the gas is seen in both emission and absorption, that is with a varying T_{BG} and requires a bright background source (e.g., [6]). Those are generally not uniformly distributed across the sky and some assumptions on the distribution of $T_S(v)$ have to made. The most common one is to assume $T_S(v)$ is constant throughout the Galaxy and often it is assumed large and the emission optically thin.

For the molecular component (H_2) the situation is more complicated. The properties of the ISM are such that H_2 has no emission lines under standard conditions and other tracers must be used. The most common used is the CO molecule that is the second most abundant one (after H_2) in the ISM, and forms under similar conditions as H_2. Additionally, the CO rotational lines are mostly excited by collisions with H_2 and the emission-line strength of the CO molecule is found to be roughly linearly related to the H_2 column density $N_{H_2}(v) \approx X_{CO}W_{CO}(v)$ [7]. Other molecular tracers such as OH can also be used but they are generally less abundant and observations more difficult.

The most frequent approach for extracting the density distribution assumes the gas is cylindrically rotating around the Galactic centre (GC, e.g., [8]). This method has been applied extensively since the beginning of systematic line emission surveys and is the basis for combined knowledge of the gas distribution in the Galaxy (e.g., reviews by [9] and [10]). As pointed out by [9], the assumption of cylindrical rotation has severe limitations because non-cylindrical streaming motions

cause significant perturbations to the observed line emission profile. In directions about the GC and anti-centre the line profiles are dominated by these streaming motions. In addition to the streaming motion, the lines are also broadened by thermal and turbulent motions of up to 10s of km s^{-1}. This velocity broadening directly affects the distance estimation and all distance estimates are broadened, causing elongated features along each line-of-sight, the so-called "fingers of god". These non-cylindrical motions make it very difficult to directly convert the line-emission surveys into 3D spatial density distributions. Some efforts have been made to correct for these inadequacies, adding elliptical motion [11] and decreased rotation for gas that is further away from the Galactic disc [12]. [13] used hydrodynamical simulation to estimate the velocity fields to get distance estimates in the direction of the GC and Gaussian profile fitting to reduce broadening. Even in that case there are noticeable artefacts from the deconvolution that smear out features in the actual spatial distribution.

In this work a different strategy is employed that uses a forward folding model fitting technique to estimate the 3D structure of the gas. By using a parametrised model continuity is enforced over the directions with limited distance information. This technique also removes the issue of artefacts caused by smearing and allows for complex gas rotation models that can also be parametrised and tuned to the data. Using a parametrised model the complexity of the spatial structure can be controlled, and it allows for a better exploration of the effect each individual modification has on the propagation of CRs.

2. Modelling the 3D gas

The parameters of the model are optimised using a maximum-likelihood fit to the H I LAB survey [14] and the DHT CO survey [15]. The survey data is re-binned to a HEALPix grid [16] using HEALPix order 7 for H I while order 8 is used for the CO data. The selected spatial resolution is mostly driven to resolve the latitudinal dependence of the gas distribution toward the GC. The velocity resolution of both surveys is degraded to 2 km s^{-1} velocity bins, which is smaller than the expected line broadening due to turbulent and thermal emotion. The statistical uncertainty on the data is assumed to be constant over the entire sky and values of 0.05 K for CO and 0.1 K for HI are assumed, which are in agreement with the noise estimate for the original surveys taking into account the re-binning. Even though the noise in the surveys is normally distributed, a student-t likelihood is used here to reduce sensitivities to large outliers that are inevitable because the model cannot capture the finest structures of the gas.

The model consists of two parts, the density of the gas $n_x(\vec{X})$ and the velocity field of the gas $\vec{v}(\vec{X})$, where $\vec{X}$ is the position in the Galaxy and the subscript x can be either H I or CO. For each line-of-sight the velocity field is used to calculate the expected Doppler shift as a function of distance to set the integration boundaries of the model. The density is then integrated along the line-of-sight and converted to line intensity. For H I the radiative transport equation is used to estimate the line intensity given an assumption for $T_S(\vec{X})$. The method can treat arbitrary forms for $T_S(\vec{X})$ but here it is assumed constant. For CO the line intensity is assumed linearly related to the density, which is suitable if the final model is turned into H_2 densities using the X_{CO} factor. To account for broadening caused by turbulent and thermal motion the models are convolved with a Gaussian kernel. The width of the kernel is chosen to be 10 km s^{-1} for the H I model and 6 km s^{-1}

for the CO model. This is in agreement with line broadening at the tangent points in the inner Galaxy.

For this contribution simple geometrical models for the density and cylindrical rotation assuming the rotation curve from [17] are used. Because the model does not provide any distance information around the GC and anti-centre the velocity information within $\pm 10^{\circ}$ longitude about both lines-of-sight is ignored and only the integrated emission is used to form the likelihood. The models are built iteratively, starting with a 2D disc model and then adding more complex features as necessary. The added features comprise: warping of the disc, a central bulge/bar, flaring in the outer Galaxy, and spiral arms. The warp and the flaring are significant only in the outer Galaxy and therefore do not have a large effect on the CO analysis that has only a small amount of gas in the outer Galaxy. The bulge/bar has only a small effect for the H I and the density ascribed to this component from the analysis is insignificant. Adding logarithmic spiral arms gives a significant improvement for both atomic and molecular gas models.

3. The 3D distribution of interstellar gas

The final model in this analysis contains 4 logarithmic spiral arms and a disc component. The spiral arms and the disc all have the same radial and vertical profile and they are both affected by a warp that is modelled with sinusoidal fluctuations[11]. The location and shape of the spiral arms is identical between the H I and CO models, but the radial and vertical profiles differ between the two. Each spiral arm also has a free normalisation in both models. In addition, the CO model has a central bulge component whose distribution is completely independent of the disc and the arms. The radial profile for the H I model consists of a spline interpolation between points at fixed radii while that for the CO model is an exponential profile with a hole in the inner Galaxy. The vertical scale height of the gas for both models increases exponentially with radius with the same radial scale length. The vertical profile of the H I model is models with $\sqrt{\mathrm{sech}(z'/z0)}$ while that of the CO model is $\mathrm{sech}^2(z'/z0)$ where z' is the vertical distance from the warped central plane of the discs and arms.

Figure 1 shows the surface density maps of the H I and CO models. The H I extends further radially than CO model, but is missing the large bulge component near the GC. The effective number of arms for the atomic and molecular gas is also different: the CO model has effectively only 3 arms because the fits prefer to assign negligible density to one, but has the other three fairly equal; the H I model has 4 arms that are split into pairs of two with the lower mass pair containing less than half the mass of the higher mass pair. The ratio of the disc mass to arm mass is also different between atomic and molecular gas models, with nearly equal mass in each part of the CO model while the H I arms account are only a quarter of the H I disc mass. The bulge is also a significant part of the CO model, accounting for about a third of the total mass. The total mass in the H I model is $\sim 5 \cdot 10^9$ Solar masses. For CO and an average X_{CO} factor of $2 \cdot 10^{20}$ cm^{-2} (K km/s)$^{-1}$ a total mass of $\sim 10^9$ Solar masses is obtained. Both values are somewhat smaller than recent estimates [4], which is to be expected because the model used here does not capture the fine structure of the Galaxy and there are significant positive residuals that can be seen in the longitude profiles shown in Figure 2. The features of the spiral arms can be easily seen in the model as sharp density enhancements. While their location is in many cases in good agreement with peaks in the

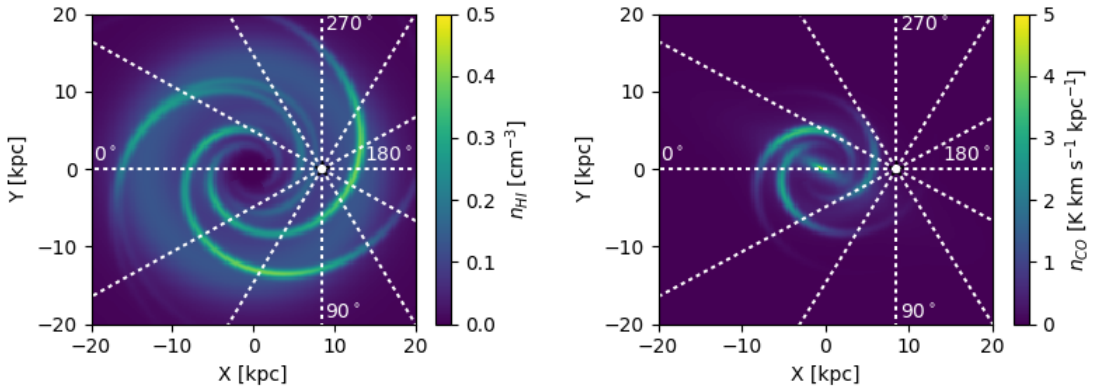

Figure 1: Surface density map of the H I (left) and CO (right) models. The geometry of the spiral arms are identical between the two models, but their radial profile and relative normalization differs. The radial extent of the H I disc is considerably larger. Lines of sight for Galactic longitudes in 30° intervals are shown as dotted lines.

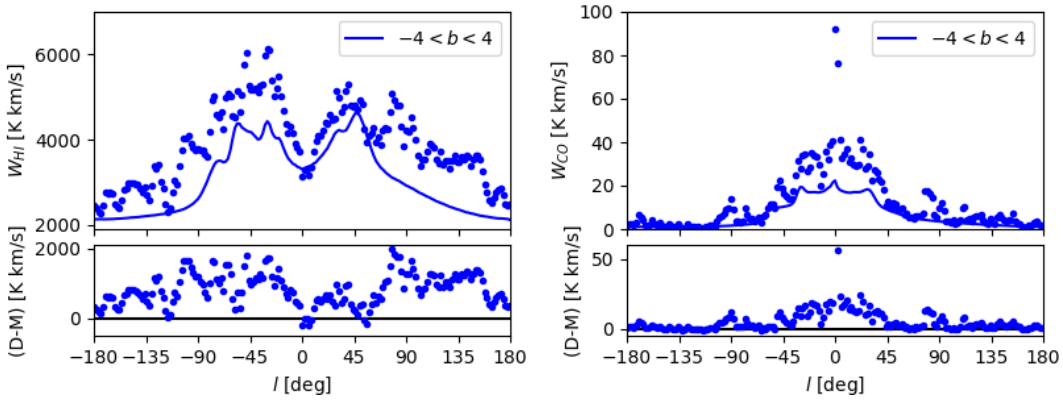

Figure 2: Longitude profiles of our gas models compared to data for H I (left) and CO (right). The models are shown as solid lines, the data as points. Both model and data are integrated over all velocities and averaged over the latitude range $-4 < b < 4$. The models roughly capture the data profiles, but departures are obvious for all latitude ranges. Note that the scale in the H I plot does not start at 0 for better contrast.

data, their magnitude is usually much smaller. There are also peaks visible in the data with no correspondence in the model, particularly for Galactic longitudes $l \sim 80°$ and $l \sim -100°$. Further freedom is therefore necessary in the models used in this work to capture the detailed distribution of the interstellar gas.

To test the effects of variations in the rotation model, ellipticity is added to the cylindrical rotation in a model without the spiral arms. This is accomplished by adding a radial component to the rotation model that varies sinusoidally with Galactic azimuth. The radial component in the optimized model has a magnitude of around 15 km s^{-1} and a maximum in the direction to the GC, in agreement with the results in [11]. The changes in rotation are also modestly in agreement with the inner Galaxy results by [18]. While the likelihood is improved with this modification to the rotation curve, the effect on the actual density model is not dramatic. There is a slight reduction in density in the inner Galaxy but an increase in the outer Galaxy. This indicates that modifying the

rotation curve in this way may not be appropriate for the inner Galaxy.

4. Effects on CR propagation

To demonstrate the effects these new models have on CR propagation we use the *GALPROP* code [19, 20, 3]. Before this work, the gas models in *GALPROP* used for the calculation of energy losses and secondary particle production were 2D asymmetric collected from the literature [21]. In addition to the new structure in the form of spiral arms and a bulge, the new models also predict more mass, $\sim$ 10% more in CO and more than double in H I. This is most likely because of larger radial extent in the new models and different vertical profiles. The average azimuthal radial distribution in the plane in the inner Galaxy is actually very similar between the new and old models.

A CR propagation model with re-acceleration and uniform diffusion is used as a test case. Two models for the gas are employed: the standard 2D azimuthally symmetric distributions in *GALPROP* that have been used successfully many times to explain CR data [22], and where the gas models are replaced with the ones described in last section. The CR source distribution is in both cases 2D azimuthally symmetric following the radial distribution of pulsars [23]. Because changing the gas models requires re-tuning of the propagation parameters the method described in [3] is followed. The propagation model parameters determined for the 2D gas model case are typical as found in other studies [22]. Using the 3D gas models produces significant changes in the propagation parameters because the total gas mass in these models is larger: the diffusion coefficient and the Alfven velocity both being about a factor of 2 lower with the new gas model. The rigidity dependence of the diffusion coefficient is similar in both models with a value that is slightly higher than the Kolmogorov $1/3$ turbulence. The source injection parameters are slightly different between the two models to account for the variations caused by the changes in propagation and energy losses. Both models agree reasonably well with CR data with differences between the two models of the order of 5% or less, mostly below few GeV .

The differences locally between the models are small by construction, but the same cannot be said for other places in the Galaxy. The change in the propagation parameters result in larger CR flux for CR primaries in the outer Galaxy, in particular at energies below few GeV. In contrast the production of secondaries is reduced in the outer Galaxy and near the GC, but enhanced near the spiral arm density structures and in general near the Sun as it is located near the edge of a minor spiral arm in the models. The result of this can be seen in Figure 3 that shows the ratio of the total γ-ray intensity of the two models at 1 GeV. The small scale structure in the ratio map is due to the gas maps used to normalize the γ-ray emission in each line of sight. The maps were identical in the two runs, all the variation is due to different emissivity calculations. The increased π^0-decay and bremsstrahlung emission in the local clouds is evident, as is the decreased emission in the outer Galaxy around 5° latitude. The decreased emission at high latitudes towards the inner Galaxy is because of reduction in IC emission that is mostly determined by the amount of primary electrons. Surprisingly, the location of the spiral arm tangent points around $l \sim 45°$, $l \sim 300°$, and $l \sim 330°$ are not standing out.

While mostly within 10%, the changes caused by the newly derived 3D gas distributions are important in the era of high-precision observations available with current instruments such as AMS-

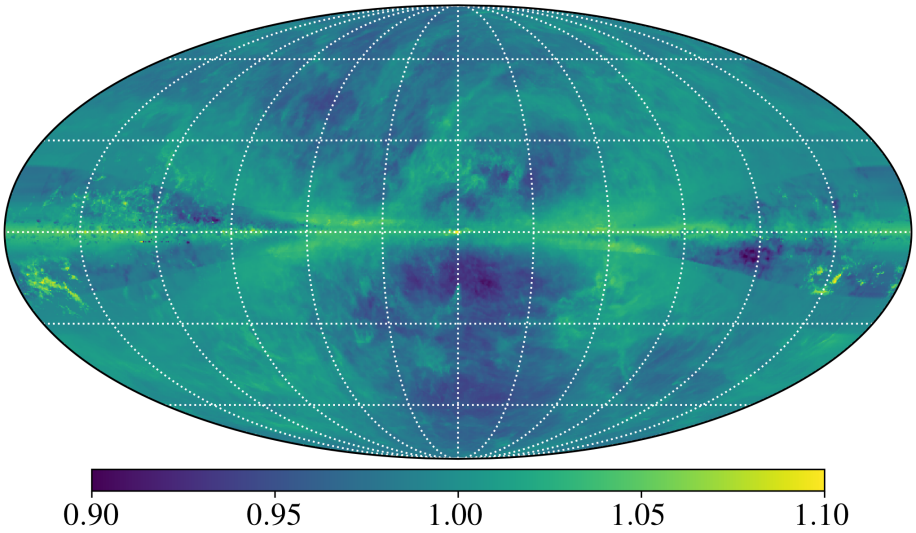

Figure 3: Ratio of the total γ-ray intensity at 1 GeV between the *GALPROP* model including the new gas models and the *GALPROP* model using the old 2D gas distributions. The map is in Galactic coordinates with the GC in the centre and longitudes increasing to the left. Graticules are spaced 30° apart.

02 and *Fermi*-LAT. Furthermore, note that the CR source density used for illustrative purposes here is 2D azimuthally symmetric. It is perfectly reasonable to expect the CR sources to follow to some extent the distribution of molecular gas that traces the star formation. Preliminary exploration of adding 3D structures to the CR source distribution is done in [3].

Acknowledgments

GALPROP development is partially funded via NASA grants NNX13AC47G and NNX17AB48G. Some of the results in this paper have been derived using the HEALPix [16] package.

References

[1] R. Schlickeiser, *Cosmic Ray Astrophysics*. 2002.

[2] A. W. Strong, I. V. Moskalenko, and V. S. Ptuskin, *Cosmic-Ray Propagation and Interactions in the Galaxy*, *Annual Review of Nuclear and Particle Science* **57** (Nov., 2007) 285–327, [astro-ph/0701517].

[3] T. A. Porter, G. Jóhannesson, and I. V. Moskalenko, *High-Energy γ-rays from the Milky Way: Three-Dimensional Spatial Models for the Cosmic-Ray and Radiation Field Densitie*, *These proceedings* (July, 2017).

[4] K. M. Ferrière, *The interstellar environment of our galaxy*, *Reviews of Modern Physics* **73** (Oct., 2001) 1031–1066, [astro-ph/0106359].

[5] S. R. Kulkarni and C. Heiles, *Neutral hydrogen and the diffuse interstellar medium*, pp. 95–153. 1988.

[6] J. M. Dickey, S. Strasser, B. M. Gaensler, M. Haverkorn, D. Kavars, N. M. McClure-Griffiths, J. Stil, and A. R. Taylor, *The Outer Disk of the Milky Way Seen in λ21 cm Absorption*, *ApJ* **693** (Mar., 2009) 1250–1260, [arXiv:0901.0968].

[7] A. D. Bolatto, M. Wolfire, and A. K. Leroy, *The CO-to-H_2 Conversion Factor*, *ARA&A* **51** (Aug., 2013) 207–268, [arXiv:1301.3498].

[8] H. Nakanishi and Y. Sofue, *Three-Dimensional Distribution of the ISM in the Milky Way Galaxy: I. The H I Disk*, *PASJ* **55** (Feb., 2003) 191–202, [astro-ph/0304338].

[9] W. B. Burton, *The structure of our Galaxy derived from observations of neutral hydrogen*, pp. 295–358. 1988.

[10] P. M. W. Kalberla and J. Kerp, *The Hi Distribution of the Milky Way*, *ARA&A* **47** (Sept., 2009) 27–61.

[11] E. S. Levine, L. Blitz, and C. Heiles, *The Vertical Structure of the Outer Milky Way H I Disk*, *ApJ* **643** (June, 2006) 881–896, [astro-ph/0601697].

[12] P. M. W. Kalberla, L. Dedes, J. Kerp, and U. Haud, *Dark matter in the Milky Way. II. The HI gas distribution as a tracer of the gravitational potential*, *A&A* **469** (July, 2007) 511–527, [arXiv:0704.3925].

[13] M. Pohl, P. Englmaier, and N. Bissantz, *Three-Dimensional Distribution of Molecular Gas in the Barred Milky Way*, *ApJ* **677** (Apr., 2008) 283–291, [arXiv:0712.4264].

[14] P. M. W. Kalberla, W. B. Burton, D. Hartmann, E. M. Arnal, E. Bajaja, R. Morras, and W. G. L. Pöppel, *The Leiden/Argentine/Bonn (LAB) Survey of Galactic HI. Final data release of the combined LDS and IAR surveys with improved stray-radiation corrections*, *A&A* **440** (Sept., 2005) 775–782, [astro-ph/0504140].

[15] T. M. Dame, D. Hartmann, and P. Thaddeus, *The Milky Way in Molecular Clouds: A New Complete CO Survey*, *ApJ* **547** (Feb., 2001) 792–813, [astro-ph/0009217].

[16] K. M. Górski, E. Hivon, A. J. Banday, B. D. Wandelt, F. K. Hansen, M. Reinecke, and M. Bartelmann, *HEALPix: A Framework for High-Resolution Discretization and Fast Analysis of Data Distributed on the Sphere*, *ApJ* **622** (Apr., 2005) 759–771, [astro-ph/0409513].

[17] Y. Sofue, M. Honma, and T. Omodaka, *Unified Rotation Curve of the Galaxy – Decomposition into de Vaucouleurs Bulge, Disk, Dark Halo, and the 9-kpc Rotation Dip –*, *PASJ* **61** (Feb., 2009) 227–236, [arXiv:0811.0859].

[18] K. Tchernyshyov and J. E. G. Peek, *Kinetic Tomography. I. A Method for Mapping the Milky Way's Interstellar Medium in Four Dimensions*, *AJ* **153** (Jan., 2017) 8, [arXiv:1611.0386].

[19] A. E. Vladimirov, S. W. Digel, G. Jóhannesson, P. F. Michelson, I. V. Moskalenko, P. L. Nolan, E. Orlando, T. A. Porter, and A. W. Strong, *GALPROP WebRun: An internet-based service for calculating galactic cosmic ray propagation and associated photon emissions*, *Computer Physics Communications* **182** (May, 2011) 1156–1161, [arXiv:1008.3642].

[20] I. V. Moskalenko, E. Jóhannesson, G. Orlando, T. A. Porter, and A. W. Strong, *GALPROP Code for Galactic Cosmic Ray Propagation and Associated Photon Emissions*, *These proceedings* (July, 2017).

[21] I. V. Moskalenko, A. W. Strong, and O. Reimer, *Diffuse galactic gamma rays, cosmic-ray nucleons and antiprotons*, *A&A* **338** (Oct., 1998) L75–L78, [astro-ph/9808084].

[22] G. Jóhannesson, R. Ruiz de Austri, A. C. Vincent, I. V. Moskalenko, E. Orlando, T. A. Porter, A. W. Strong, R. Trotta, F. Feroz, P. Graff, and M. P. Hobson, *Bayesian Analysis of Cosmic Ray Propagation: Evidence against Homogeneous Diffusion*, *ApJ* **824** (June, 2016) 16, [arXiv:1602.0224].

[23] I. Yusifov and I. Küçük, *Revisiting the radial distribution of pulsars in the Galaxy*, *A&A* **422** (Aug., 2004) 545–553, [astro-ph/0405559].